

Imprints of recoiling massive black-holes on the hot gas of early type galaxies

B. Devecchi¹, E. Rasia^{3,4}, M. Dotti², M. Volonteri², M. Colpi¹

¹ *Dipartimento di Fisica G. Occhialini, Università degli Studi di Milano Bicocca, Piazza della Scienza 3, 20126 Milano, Italy*

² *Dept. of Astronomy, University of Michigan, Ann Arbor, MI 48109, USA*

³ *Dept. of Physics, University of Michigan, Ann Arbor, MI 48109, USA*

⁴ *Chandra Fellow*

1 November 2018

ABSTRACT

Anisotropic gravitational radiation from a coalescing black hole binary is known to impart recoil velocities of up to $\sim 1000 \text{ km s}^{-1}$ to the remnant black hole. In this context, we study the motion of a recoiling black hole inside a galaxy modelled as an Hernquist sphere, and the signature that the hole imprints on the hot gas, using N-body/SPH simulations. Ejection of the black hole results in a sudden expansion of the gas ending with the formation of a gaseous core, similarly to what is seen for the stars. A cometary tail of particles bound to the black hole is initially released along its trail. As the black hole moves on a return orbit, a nearly spherical swarm of hot gaseous particles forms at every apocentre: this feature can live up to $\approx 10^8 \text{ yr}$. If the recoil velocity exceeds the sound speed initially, the black hole shocks the gas in the form of a Mach cone in density near each super-sonic pericentric passage. We find that the X-ray fingerprint of a recoiling black hole can be detected in *Chandra* X-ray maps out to a distance of Virgo. For exceptionally massive black holes the Mach cone and the wakes could be observed out to a few hundred of Mpc. Detection of the Mach cone is found to become of twofold importance: i) as a probe of high-velocity recoils and ii) as an assessment of the scatter of the $M_{\text{BH}} - M_{\text{bulge}}$ relation at large black hole masses.

Key words:

1 INTRODUCTION

Today, black holes (BHs) with masses in excess of $10^6 M_{\odot}$ appear to be ubiquitous in bright galaxies (Richstone et al. 1998; Decarli et al. 2007) and scaling relations between the BH mass and the underlying galaxy indicate unambiguously that BHs evolve in symbiosis with their hosts (Ferrarese & Merritt 2000; Gebhardt et al. 2000; Hopkins et al. 2006).

According to the current paradigm of structure formation, galaxies often interact and merge as their dark matter halos assemble in a hierarchical fashion, and the BHs, incorporated through mergers, are expected to grow, evolve and *pair* with other BHs (Volonteri et al. 2003). The formation of super-massive BH pairs thus appear to be an inevitable and natural consequence of galaxy assembly.

In our local universe, the dual radio source 3C 75, at the centre of Abell 400, is a clear, albeit rare example of BH pairing as it hosts two massive BHs displaying prominent radio jets (Owen et al. 1985). *Chandra* observations of 3C 75 have revealed the occurrence of two active nuclei at a projected separation of 7 kpc (Hudson et al. 2006) providing first ev-

idence of their current coupling. An even more remarkable, and still unique example is the case of the elliptical galaxy 0402+369 (Rodriguez et al. 2006). VLBI observations highlighted the presence of two compact variable, flat-spectrum radio sources at a projected separation of only 7 pc, suggesting that the two massive BHs that power the radio emission form a *binary*. These two cases indicate that BH pairing occurs and proceeds from the large-scale of a merger (up to 100 kpc) down to the scale where the BHs form a binary in close Keplerian relative orbit (of a few pc). In the interaction with the stars (Milosavljević & Merritt 2001; Yu 2002; Berczik et al. 2006; Merritt & Milosavljević 2005; Sesana et al. 2007) and/or gas (Armitage & Natarajan 2002; Escala et al. 2004; Escala et al. 2005; Dotti et al. 2006; Dotti et al. 2007; Mayer et al. 2007) that surround the binary, the BHs lose orbital angular momentum, and if the process continues down to a scale of a few milliparsec, gravitational wave emission drives the BH in-spiral down to coalescence, causing the formation of an heavier *remnant* BH.

Recently, a major breakthrough in numerical relativity

has allowed to trace for the first time the BH binary evolution down to coalescence (Pretorius 2007), in the *strong field* regime imposed by general relativity under arbitrary conditions (Campanelli et al. 2007A; Campanelli et al. 2007B; Bruegmann et al. 2007; Baker et al. 2007; Baker et al. 2008; Herrmann et al. 2007; Herrmann et al. 2007; Herrmann et al. 2007; Koppitz et al. 2007). These studies have revealed that spinning BHs emit an anisotropic beam of gravitational radiation, and in response to this asymmetry the remnant BH receives a *recoil* (due to linear momentum conservation) that can displace it from the central parts of the galaxy. In more detail, BHs with similar masses and spin vectors in non-generic alignments relative to the orbit produce anisotropic patterns of radiation via spin-orbit coupling that lead to recoil velocities v_{rec} in the range of $\lesssim 200 \text{ km s}^{-1}$ to 2000 km s^{-1} , and for particular spin-orbit configurations to a recoil as high as 4000 km s^{-1} (Campanelli et al. 2007A; Campanelli et al. 2007B; Baker et al. 2008; Schnittman & Buonanno 2007). These “natal kicks” are in the range of the typical dispersion/rotation velocities of galaxies or even higher, so that the remnant BH can either be significantly displaced away from the galactic centre where the merger occurred, or be ejected when v_{rec} exceeds the escape speed from the galaxy (typically of $\sim 1000 \text{ km s}^{-1}$ for massive galaxies).

Both a BH that remains or a BH that escapes can leave a “sign” on the underlying galaxy with observable consequences. As an example, a BH ejected from its host galaxy can carry a punctuated accretion disc that lights the BH on, as an active X-ray source, eventually deprived of its underlying galaxy (Loeb 2007). Can a BH retained in the galaxy carry other observable features? This is the question that we address in this paper.

A kicked BH, retained inside the host galaxy, moves along a radial elongated orbit; it both explores the galaxy periphery and cross the centre a few times, periodically. Dynamical friction against stars and gas causes its radial orbit to decay over a time-scale that depends on the recoil velocity and underlying background density.

The BH damped oscillatory motion, in a pure stellar background, has been investigated by a number of authors (Merritt et al. 2004; Boylan-Kolchin et al. 2004; Gualandris & Merritt 2007). After an early phase of braking under the action of dynamical friction and a number of recursive passages across the centre of the galaxy, the orbital decay cause the motion of the BH to be confined into its gravitational influence radius. From this point on the BH starts oscillating together with the core around the common centre of mass and it eventually reaches thermal equilibrium with the stars when the oscillations decays down to Brownian level (Gualandris & Merritt 2007).

The interaction of the massive BH with stars has no negligible effects on the underlying equilibrium (Boylan-Kolchin et al. 2004; Merritt et al. 2004; Gualandris & Merritt 2007), the most interesting being the formation of a *stellar core*. As pointed out by Boylan-Kolchin et al. (2004), the instantaneous removal of the BH from the galaxy centre, at the time of its ejection, causes a sudden decrease in the gravitational potential so that stars driven away from virial equilibrium respond dynamically expanding. In addition, when the BH returns to the centre, it transfer orbital kinetic energy into

the background under the action of dynamical friction, and this energy deposition causes further stellar expansion.

In this paper we address a complementary problem, i.e. the effect that a recoiling BH has on the hot gaseous component of an early type galaxy host. Local temperature and density perturbations excited by the super-massive BH while it is travelling across the galaxy are expected to lead to observable changes of the bremsstrahlung emission. We will specifically address the following issues i) how the structural properties of the gas in the galaxy are modified by the ejection of the BH and its orbital decay; ii) which signatures the BH motion imprints on the gas; iii) the prospects for detection of these signatures by X-ray telescope such as Chandra.

For this study, we perform a suite of 8 simulations of gas rich elliptical galaxies, where BHs are ejected with different recoil velocities. The BH mass M_{BH} scales with the host mass according to the observed correlation (Häring & Rix 2004). Since this correlation has an intrinsic scatter of at least 0.3 dex (see Lauer et al. 2007, Tundo et al. 2007 for a discussion of the scatter of the correlations at large BH masses), we also study the case of an over-massive BH with a mass a factor of 3 larger than predicted by the best fit value of the $M_{\text{BH}} - M_{\text{bulge}}$ relation in Häring & Rix (2004).

The outline of the paper is as follows. In Section 2 we introduce the physical model used in our simulations. In Section 3 we describe the changes in time of the density and temperature induced by the ejected BH, inferred considering different recoil velocities, and for a BH mass following the $M_{\text{BH}} - M_{\text{bulge}}$ relation and its scatter. In Section 4, we explore the BH detectability with *Chandra*. In Section 5 we discuss our results.

2 SIMULATIONS

We perform our simulations using the N-Body/SPH code GADGET (Springel et al. 2001). The elliptical galaxies are modelled as an Hernquist sphere (Hernquist 1990) with scale radius a and total mass M_{tot} . The mass density, cumulative mass profile and escape velocity are given by:

$$\rho(r) = \frac{M_{\text{tot}}}{2\pi} \frac{a}{r(r+a)^3} \quad (1)$$

$$M(r) = M_{\text{tot}} \frac{r^2}{(r+a)^2} \quad (2)$$

$$v_{\text{esc}} = (2GM_{\text{tot}}/a)^{1/2}. \quad (3)$$

The total mass of the galaxy is $M_{\text{tot}} = 10^{12} M_{\odot}$, with a gas fraction $f_{\text{gas}} \equiv M_{\text{gas}}/M_{\text{tot}} = 0.1$; the gas follows the same density profile of the stellar component. We explore two different scale radii: a equal to 4 and 8 kpc, and two different BH masses, 2 and $6 \times 10^9 M_{\odot}$ (see Table 1). The lightest BH follows the $M_{\text{BH}} - M_{\text{bulge}}$ relation as in Häring & Rix (2004), while the heaviest explores the scatter at high BH masses (Lauer et al. 2007, Tundo et al. 2007) where we expect the imprints of the recoils to be the largest.

For the collisionless component we use 10^5 particles with a gravitational softening of 100 pc to prevent numerical collisional relaxation. In the runs with the light (heavy) BH we use 2×10^6 (10^6) gaseous particles with softening

$h_{\text{gas}} = 10$ (50) pc; the number of gas particles used to average the hydrodynamical properties is 40, so that our mass resolution is $\approx 2 \times 10^7 M_{\odot}$ ($10^7 M_{\odot}$). Each gaseous particle is evolved along a polytrope $P \propto \rho^{\gamma}$ with $\gamma = 5/3$, corresponding to adiabatic evolution of an ideal gas. Compressional work and shock heating are included in the energy equation. The gravitational softening of the BH equals that of the gas, $h_{\text{BH}} = h_{\text{gas}}$. We ensure that the dynamical influence of the hole on the gas is resolved, by checking that $h_{\text{BH}} \ll r_{\text{inf}} \simeq a(2M_{\text{BH}}/M_{\text{tot}})^{1/2}$. Here the influence radius, r_{inf} is defined as the distance from the galaxy centre that encloses a total mass equal to $2M_{\text{BH}}$. For the less massive BH:

$$r_{\text{inf}} \simeq 253 \left(\frac{a}{4 \text{ kpc}} \right) \left(\frac{M_{\text{BH}}}{2 \times 10^9 M_{\odot}} \frac{10^{12} M_{\odot}}{M_{\text{tot}}} \right)^{1/2} \text{ pc.} \quad (4)$$

We set the initial condition for the BH plus galaxy system following the prescription by Hernquist (1993), and we evolve the equilibrium model for 1 Gyr to verify its stability. After the ejection, we halt our simulations when the BH has settled into its Brownian motion.

We explore the ejection of the BH for different recoil velocities v_{rec} ranging from 0.2 to 0.95 the escape velocity, v_{esc} . In the simulations with $a = 4$ (8) kpc the escape velocity at $r = 0$ is 1490 (1054) km s^{-1} and the central initial sound speed is 400 (300) km s^{-1} . The resulting initial Mach number, defined as $\mathcal{M} \equiv v_{\text{rec}}/c_{s,0}$ ranges between 1 and 3.3. Table 1 lists physical parameters for all 8 models: a, through H. We will identify with lower-case (upper-case) letters the runs referring to the light (heavy) black hole.

3 BH INTERACTION WITH THE HOT GAS

The recoiling BH reaches its first apocentre $r_{\text{apo}} \sim a [(1 - v_{\text{rec}}^2/v_{\text{esc}}^2)^{-1} - 1]$. Following the kick, the motion of the BH exhibits three distinct phases: (i) a decaying oscillatory radial motion guided by dynamical friction; (ii) a phase characterised by BH oscillations well inside the galaxy scale radius followed by (iii) Brownian motion. These phases agree with what Gualandris & Merritt (2008) found for the collisionless case.

In the following we investigate the direct influence that the ejection of the BH has on gas density and temperature, looking at the evolution of both radial profiles and 2-dimensional maps.

3.1 Density and temperature radial profiles

We now turn our attention to the global disturbance that the BH imprints on the gas. We first focus on a simulation with $M_{\text{BH}} = 2 \times 10^9 M_{\odot}$ (run b, $\mathcal{M} = 3$), and analyse how the density and temperature profiles change during the entire run. In run b the orbit decays into the Brownian regime after ~ 458 Myr (i.e., $\sim 20 t_{\text{dyn}}$ where $t_{\text{dyn}} = (3\pi^2 a^3 / (GM_{\text{tot}}))^{1/2}$).

Figure 1 shows the evolution of the radial density profile. When the BH is at its first apo-centre (22 Myr after the ejection) the central density drops creating a core within $\approx 2r_{\text{inf}}$. The density keeps decreasing until the BH sets

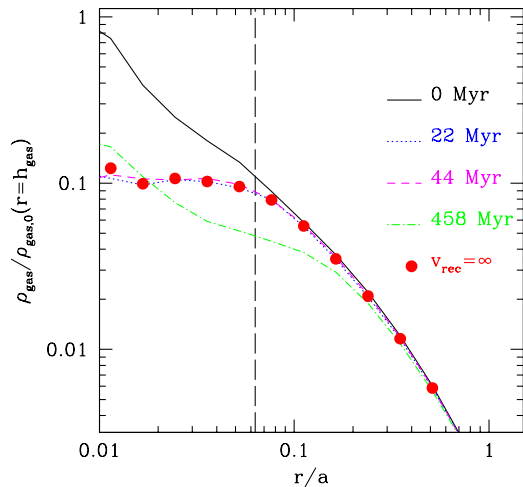


Figure 1. Radial density profiles of gas, in units of the initial central density at the softening radius, as a function of the distance from the centre of the galaxy in units of a for run b at different times. Solid line refers to the initial condition, dotted and dashed lines to the time at which the BH is at its first apocentre and first pericentre respectively. Dot-dashed line refers to the final configuration when the BH orbit has decayed. Vertical line indicates the position of r_{inf} . Red dots refers to the run g where the BH have been instantaneously removed.

into its Brownian motion. The final central gas density is $\approx 9 - 10$ times lower than the initial value, and the final gaseous core has a size $\approx 4r_{\text{inf}}$.

The evolution of the radial density profile is caused by the same two processes outlined by Boylan-Kolchin et al. (2004) and Merritt et al. (2004) for the stellar component. At first the density drop is due to the sudden removal of the BH gravitational field and not to dynamical friction: in response to this change, the stellar and gaseous components readjust to a dynamical equilibrium state with no BH. To check this hypothesis we carried out a test simulation where the BH was removed instantaneously from the galaxy (run g for $M_{\text{BH}} = 2 \times 10^9 M_{\odot}$) and we let the system evolve for 22 Myr. Density profiles for run b and run g at this time are indeed very similar, confirming this initial hypothesis. At later times, the density evolution is driven by dynamical friction, which injects energy into the background at each supersonic pericentric passage. When the orbital decay is completed, the combined action of the two processes ends with an erosion extending all the way to $4r_{\text{inf}}$.

Figure 2 shows the evolution of the temperature profile in run b. The central temperature T decreases in response to the ejection of the BH as well. However, when the BH settles down in its Brownian motion, T returns to its virial value.

The final gas density profiles normalised to the initial profiles are shown in Figure 3 for cases from a through F. Core formation occurs in all cases. For a fixed M_{BH} , the importance of the core increases with v_{rec} , while for a fixed

Run	M_{BH}	v_{esc}	v_{rec}	\mathcal{M}	$M_{\text{def,star}}/M_{\text{BH}}$	$M_{\text{def,gas}}/M_{\text{BH}}$	$M_{\text{def,tot}}/M_{\text{BH}}$	r_{core}/a	$M_{\text{gas,b}}/M_{\text{BH}}$
a	2	1490	500	1.3	1	0.24	1.24	0.16	0.13
b	2	1490	1200	3	3.2	0.63	3.83	0.35	0.01
C	6	1054	400	1.3	1.8	0.19	2.	0.16	0.3
D	6	1054	700	2.3	3.5	0.35	3.85	0.275	0.1
E	6	1054	900	3	3.8	0.43	4.2	0.36	0.061
F	6	1054	1000	3.3	4.	0.53	4.5	0.41	0.05
g	2	1490	∞	∞	0.73	0.06	0.79	0.075	-
H	6	1054	∞	∞	1.53	0.21	1.75	0.19	-

Table 1. List of the simulations: label of the run; BH mass in unit of $10^9 M_{\odot}$; escape velocity at $r=0$ and initial recoiling velocity in km s^{-1} ; initial Mach number \mathcal{M} ; mass deficit in stars, gas and their sum in units of M_{BH} ; core radius in unit of scale radius, a ; mass of particles initially bound to the BH $M_{\text{gas,b}}$ in units of M_{BH} . Run g and H correspond to the case of instantaneous removal of the BH. In run a, b, g (C, D, E, F, H) the scale radius is equal to 4 (8) kpc and the initial sound speed is 400 (300) km s^{-1} .

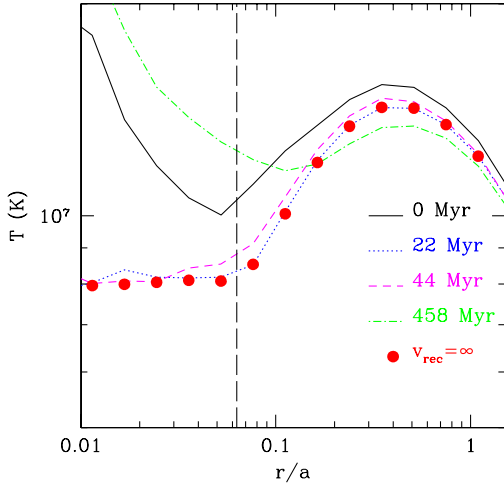


Figure 2. Radial temperature profiles of gas as a function of the distance from the centre of the galaxy in units of a for run b at different times. Solid line refers to the initial condition, dotted and dashed lines refer to the first apocentre and pericentre, respectively. Dot-dashed line refers to the final configuration. Vertical line indicates the position of r_{inf} .

v_{rec} it increases for more massive BHs, i.e., with the kinetic energy deposited by the BH. For low recoil velocities ($\mathcal{M} \sim 1$), the kinetic energy carried by the BH and deposited in its transit across the centre of the galaxy is low, and the major perturbation acting on the gas is related to the temporary removal of the BH at the time of coalescence.

We compute final core radii, and mass deficits both for the gaseous ($M_{\text{def,gas}}$) and stellar ($M_{\text{def,star}}$) components (see Table 1). $M_{\text{def,star}}$ is always larger than $M_{\text{def,gas}}$, because in all our simulations the stellar mass is larger compared to the gaseous one. The total, star+gas, deficits span from 1.5 up to 4 M_{BH} , in agreement with the results from collisionless simulations (Boylan-Kolchin et al. 2004; Guandris & Merritt 2007; Merritt et al. 2004).

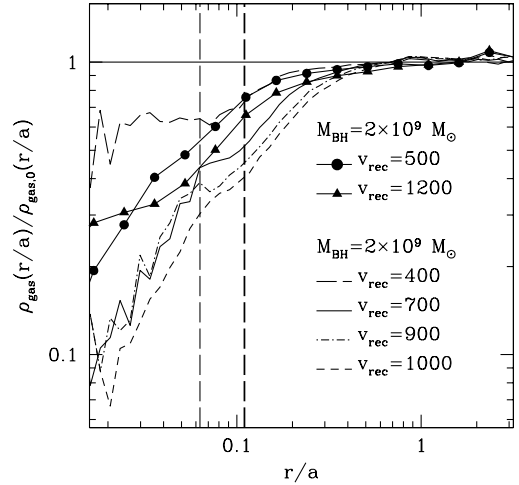


Figure 3. Final gas density profiles ρ_{gas} as function of r/a , normalised to the density profile at $t=0$ $\rho_{\text{gas},0}$ for the two sets of run with different BH masses and different recoil velocities v_{rec} (in units of km s^{-1}). Vertical lines refer to the influence radii of the two BH masses: light (heavy) curve for $M_{\text{BH}} = 2 (6) \times 10^9 M_{\odot}$.

3.2 Density and temperature 2-D maps

In this section we study the shape and extent of the density and temperature perturbations that the BH excites along its trail. We first discuss models with $\mathcal{M} \simeq 1$, i.e. run a and C. During the orbital decay the BH is always surrounded by a hot spherical over-density of gaseous particles. The size of the spherical overdensity corresponds roughly to $r_b \equiv GM_{\text{BH}}/v_{\text{rec}}^2$, i.e. the radius within which particles remain bound after the BH is kicked. The density enhancement is illustrated in the upper panels of Figure 4 for both runs when the BH is at its first apocentre.

Another characteristic feature in the density maps of these early dynamical phases, is a stream of gas particles lagging behind the BH trail. We argue that this gas is stripped material initially residing inside r_{inf} . To test this hypothesis

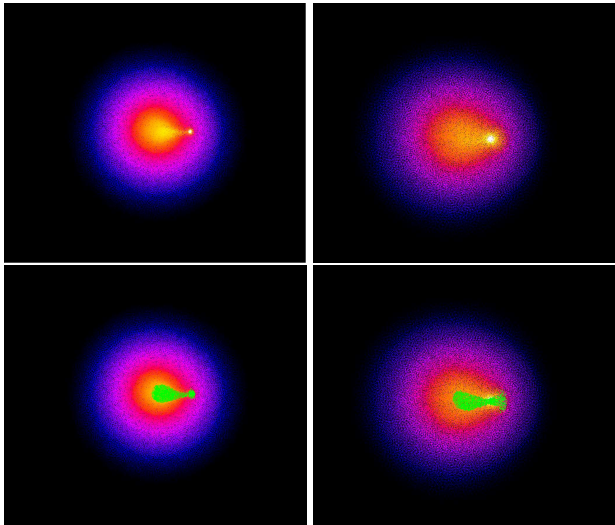


Figure 4. Upper panel: color-coded gaseous density maps in logarithmic scale for run a (left) and C (right) ($v_{\text{rec}} = 500 \text{ km s}^{-1}$ and 400 km s^{-1} , respectively) when the BH is at its first apocentre. Brighter colors refer to higher densities that range between 0.1 and 10^{-3} cm^{-3} . Lower panel: same maps but where the gaseous particles initially bound to the BH are marked in green. Boxes are $2a$ on a side (i.e. 8 and 16 kpc for run a and C, respectively). The BH initial orbit is on the x-axis and maps are projected in the x-y plane

we mark, at the start of runs a and C, the particles gravitationally bound to the BH¹, and then follow their dynamics. Figure 4 shows the density map of the gas surrounding the BH at its first apocentre. In the lower panels the particles originally bound to the BH are marked in green. Here a clear spatial coincidence between the stream and the marked particles appears, thus supporting our hypothesis.

As we move to higher velocities ($\mathcal{M} > 2$), the mass of particles initially bound to the recoiling BH ($M_{\text{gas,b}}$) decreases considerably as reported in Table 1. Again, this was previously noted for the stellar case by Gualandris & Merritt (2008). The quasi spherical swarm of hot gaseous particles around the BH becomes less relevant, and for the case with the highest speed (runs b and F), it is no longer visible even soon after the ejection. The lack of particles around the BH for large Mach numbers is a consequence of our resolution limits: for kick velocities $\gtrsim 800 \text{ km s}^{-1}$ (700 km s^{-1}) and for the light (heavy) BH, the radius r_b drops below our resolution limit so that we are unable to resolve the initially bound particles anymore.

New features appear when $\mathcal{M} > 2$ initially: a steep, conical over density develops, i.e. a Mach cone becomes visible in the density maps, as shown in Figure 5. The opening angle of the cone is inversely proportional to \mathcal{M} , and varies along the BH trajectory as both its speed and background temperature vary. The shape of the cone is sharpest at the first pericentre passage, where the contrast between the speed of

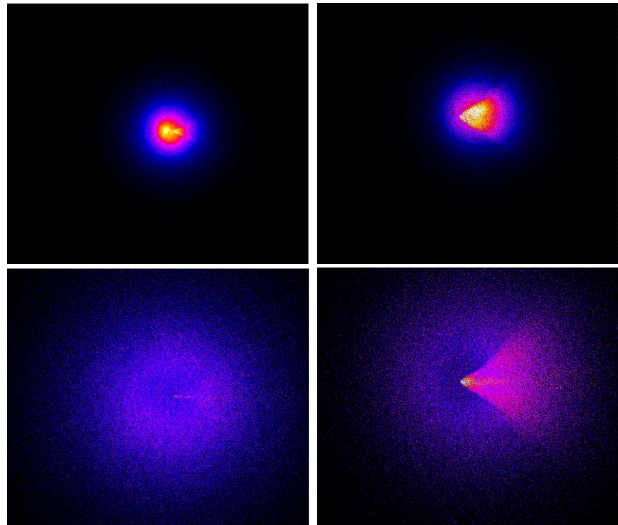


Figure 5. Upper panel: color-coded gaseous density maps in linear scale for run b (left) and E (right) with $\mathcal{M} = 3$ when the BH is at its first pericentre. Density range between 0.001 and $0.05 \text{ cm}^{-3} q$. Lower panel: color-coded temperature map in logarithmic scale between $5 \times 10^6 \text{ K}$ and $1.5 \times 10^7 \text{ K}$. Boxes are 4 and 20 kpc on a side for run b and E, respectively. The BH initial orbit is on the x-axis and maps are projected in the x-y plane

the perturber and the temperature of the gas is the highest (see Figure 2). The cone then weakens during the rest of the simulation as dynamical friction slows down the BH motion, and the temperature returns to its virial value. The Mach cone is clearly visible along the direction orthogonal to the BH velocity vector, and it can still be recognisable as long as the angle between the line of sight and the BH is below ~ 45 degrees.

All these features are transient and have a characteristic lifetime that depends on the BH-galaxy mass ratio, on the extent of the recoil velocity imparted at the moment of BH coalescence, and on the background. For low Mach numbers, $\mathcal{M} \sim 1$, the over-density around the BH is more easily visible when the BH is at apocentre as the density and temperature contrast with the background are the highest. As the BH spends most of the time at apocentre, this over-density can be observed for $10 - 100 \text{ Myr}$. For high Mach numbers, i.e. recoil velocities near escape, the Mach cone becomes the main feature and it is seen during the first supersonic pericentres close to the central region of the host galaxy, within a scale ranging between $0.5-2 \text{ kpc}$. The corresponding lifetime is a few tens of Myr.

3.3 Gas fraction

We now briefly discuss how the density and temperature perturbations excited by the BH travelling across the hot gas of the galaxy depend on the fraction of gas f_{gas} relative to the stellar mass. Although we have modelled gas rich early type galaxies with $f_{\text{gas}} = 0.1$, the dynamical evolution of the BH is still dominated by the stellar component. As a consequence, a further reduction of f_{gas} does not alter the BH orbit or the characteristic decay time. As the gas is in virial equilibrium, its sound speed and temperature

¹ We define particles gravitationally bound to the BH as done in Gualandris & Merritt (2008): we calculate the relative energy between the BH and each particle. When this energy is negative we define the particle as bound to the BH.

are determined by the overall gravitational potential, and thus do not vary for smaller f_{gas} . Since the shape of the perturbation depends on the value of the Mach number and on the size of the BH influence radius, galaxy models with different gas fractions but same \mathcal{M} and M_{BH} , differ only in the total X-ray luminosity (discussed in Section 4). We run a test simulation with $f_{\text{gas}} = 0.01$, $\mathcal{M} = 2.3$ and $M_{\text{BH}} = 6 \times 10^9 M_{\odot}$ to verify these scaling and find good agreement with our expectations.

4 DETECTABILITY

The motion of the BH perturbs the density and temperature distribution. Bremsstrahlung emission from the perturbed gas is expected to create X-ray features above the diffuse emission from the underlying hot gas in the galaxy. In this Section, we quantify the detectability of signatures related to recoiling BHs in X-rays. We create synthetic *Chandra* observations using the code X-ray MApp Simulator (Gardini et al. 2004; Rasia et al. 2008, X-MAS). The mock event files are generated in the soft band, [0.7, 2] keV, assuming the Response Matrix File and the Ancillary Response File of the *Chandra* detector ACIS-S 3. The images are created assuming an exposure time of 10 ks for the heavy BH and 100 ks for the light BH. The galaxy-BH system is considered to be at the distance of Virgo ($z=0.004$), meaning that the field of view of our detector (8.3 arcmin) corresponds to 42 kpc. The orbital plane of the BH is perpendicular to the X-ray image and oriented along the horizontal axis unless otherwise noted.

The drop in central density is less dramatic for the light BH and the swarm of bound particles less evident. The X-ray contrast of the features produced over the underlying galaxy is consequently weaker than in runs with a heavy BH. Identification of recoil signatures on raw surface brightness maps is hard. To better highlight the influence of the BH in *Chandra* maps and to quantify its relevance over the background galaxy, we create “mirror images”. We rotate a galaxy image by 180 degrees around the axis orthogonal to the BH motion and then divide the original image by the rotated one (this technique is reminiscent of the “Asymmetry” index used in optical astronomy, e.g., Conselice 2003).

Selected *mirror images* for the light BH are shown in Figure 6. When $\mathcal{M} = 1$ (run a), the perturbation of the gas results in an X-ray enhancement off-set relative to the galaxy centre. Its concentration and spherical shape can be associated to the feature outlined in Figure 4. The three images for run b represent three different moments of the BH orbital decay. During the first oscillations the BH has an orbit with large radii (~ 8 kpc). The residues of its passage are visible, as broad wings, up to 5 kpc from the centre. As the decay proceeds the orbital radius decreases and in this particular simulation the BH starts to precess after ~ 200 Myr. The second mirror image is taken after 266 Myr when the motion axis is tilted by almost 45 degrees respect to its original orientation. Here the BH motion is traced by the two yellow spots oriented along the BH trajectory. The last image refers to the last phase of the BH motion when the BH moves in a short orbit across the centre and passes frequently through the same excited region. The X-ray enhancement increases the background emission of 30%.

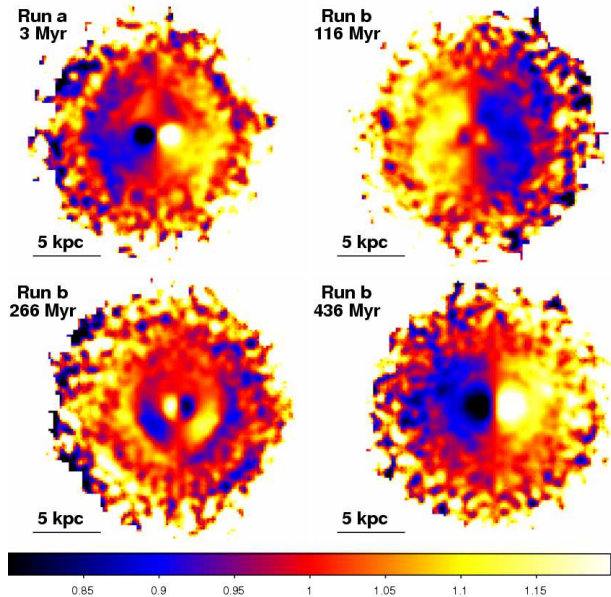


Figure 6. Mirror images for the light BH smoothed with a gaussian filter. Left-Top panel: Run a, when the BH is in its first apocentre. Right-Top, Left-Bottom and Right-Bottom panel: Mirror images for run b at three different moments of the BH motion (time after the ejection are shown in each panel). The color scale is linear between 0.8 and 1.2.

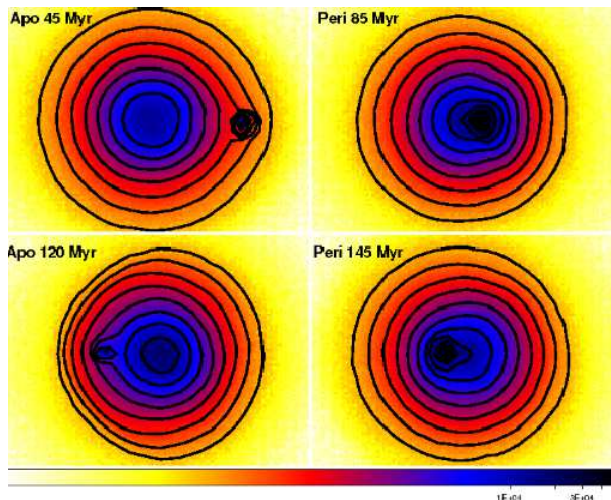


Figure 7. Simulated color coded maps of the X-ray emission detectable by *Chandra* (ACIS-S3 chip), for run D. The photon images are computed in the [0.7 2] keV band, background subtracted and 1 arcsec binned. The angular size is 2.7 arcmin corresponding approximately at 14 kpc at the source redshift ($z=0.004$). The scale is logarithmic and the isophotal contours (shown in black) are logarithmically equi-spaced between 100 and 50000. Different panels correspond to first apocentric phases (denoted by Apo) and pericentric ones (denoted by Peri). The last pericentre showed is after 145 Myr, while the last apocentre is at 120 Myr.

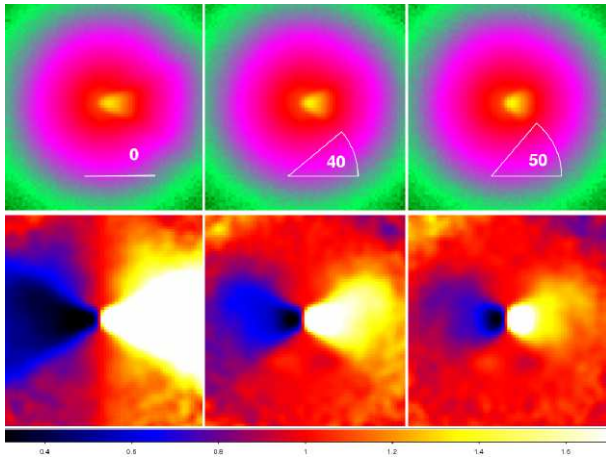


Figure 8. Upper panels: Simulated color coded maps of the X-ray emission detectable by *Chandra* (ACIS-S3 chip), for run E for different angles (reported in each image) between the plane orthogonal to the line of sight and the BH motion. Lower panels: Mirror images for run E (with the heavy BH) smoothed with a gaussian filter for different rotation angles between the line of sight and the BH motion. The color scale is linear between 0.3 and 1.8. The angular size in all images is 2 arcmin corresponding approximately at 10 kpc at the source redshift ($z=0.004$).

4.1 Detectability of “outliers”

As already mention, the heavier the BH with respect to its host, the stronger the thermodynamical perturbations are. We recall that “heavy” in this context means that the BH is above the $M_{\text{BH}} - M_{\text{bulge}}$ relation (i.e. an “outlier”).

A heavier BH perturbs the background more strongly. Figure 7 shows photon images of the X-ray emission detectable by *Chandra*, for run D. In this case the presence of the BH results not only as a clear distortion of the iso-photal contours, but also as a peaked emission separate from the centre. This spherical X-ray enhancement survives for many passages through the centre. In Figure 8 we clearly distinguish the strong feature of the Mach cone for run E. The mirror images, in this case, present sharp well defined edges limiting the Mach cone which reaches a maximum contrast of 300% over the background. The first panel shows the X-ray images when the cone axis is aligned with the horizontal axis. It is important to asses if the features are visible along lines of sight non exactly orthogonal to the BH motion. We produce maps where the angle between the cone axis and the plane orthogonal to the line of sight increases from 0 (the reference value) to 60 degrees in steps of 5 degrees. The signature is recognisable as a cone when the angle is below 45 degrees, in good agreement with the result we found for the density 2D maps alone. For angle above 45 degrees we still detect a strong inhomogeneity but the cone structure is lost.

Chandra can resolve the wake of “outliers” to a greater distance and in smaller galaxies. The Mach cone is not only a key feature for revealing a moving BH with high recoil velocities, but it also highlights the presence of an outlier. In the following, we rescale our results to galaxies with smaller gas fraction and to smaller galaxies, in both cases hosting massive BHs above the $M_{\text{BH}} - M_{\text{bulge}}$ relation, “outliers”.

We first consider how the observability of the conical wake depends on the gas fraction. As discussed above, the dynamical evolution of the BH is mainly driven by the interaction with stars, so that the shape of the X-ray features is a function only of the properties of the recoiling BH. In galaxies with a smaller gas fraction it is only the total X-ray flux that changes.

In order to determine if the wake is visible relative to the background galaxy, the corresponding signal to noise² ratio (S/N) needs to be greater than a given detectability threshold. The counts expected from a *Chandra* observation of 10 ks give values of the S/N ratio greater than 10 for gas fractions above $f_{\text{gas}} = 10^{-3}$, reassuring that, at the distance of Virgo, $\sim 10^9 M_{\odot}$ BHs ejected with supersonic velocity are all detectable.

We now consider the sensitivity of our results to the size of the galaxy. Our simulations are scale-free, as long as the units we use are consistent with the same gravitational constant adopted in GADGET to evolve the system. If we scale the masses ($M' = \alpha M$), the radii need to be rescaled ($R' = \alpha^{0.56} R$, see Shen et al. 2003) in order to preserve the relationship between the scale radius and the mass of the galaxy: accordingly the time follows $t' = \alpha^{0.34} t$. For the new system the luminosity of the bremsstrahlung emission is related to the old one by $L' = \alpha^{0.54} L$.

In order to determine the minimum value of α for which we can still observe the wake, we have to take into account not only the S/N ratio, but also the angular resolution of *Chandra*. For our reference galaxy the maximum radius of the wake in run b at the first pericentre is ≈ 2 kpc. We consider the wake in a galaxy at a distance d as resolved by *Chandra* if the angular extent of the wake is covered by 4 resolution elements (0.5 arcsec, i.e. the angular resolution of the telescope). For galaxies at distances comparable the Virgo cluster the critical α for a wake to be resolved is $\alpha_{\text{lim}} \sim 8 \times 10^{-3}$, corresponding to a BH mass greater than $\sim 5 \times 10^7 M_{\odot}$. Fixing α_{lim} we have carried on the same analysis outlined above for $f_{\text{gas}} = 0.1, 10^{-2}$ and 10^{-3} . For $f_{\text{gas}} = 0.1$ and 10^{-2} the ratio of S/N is again greater than 10. For $f_{\text{gas}} = 10^{-3}$ it drops to 2 only.

What happens if we consider more distant galaxies? The resolution of *Chandra* would allow to resolve the wake in our reference galaxy up to a distance of ~ 300 Mpc. The minimum value of α is related to the distance d by $\alpha \sim 8 \times 10^{-3} (d/20 \text{ Mpc})^{1/0.56}$. The detection limits imposed by the S/N ratio are less tight than those given by the requirement on the spatial resolution unless $f_{\text{gas}} < 10^{-2}$.

5 SUMMARY AND DISCUSSION

In this paper we studied the perturbation that a recoiling massive BH can imprint on the hot gaseous component of its host elliptical. The BH is able to affect not only the stellar component (as previously noted by Boylan-Kolchin et al. (2004) and Gualandris & Merritt (2008)), but also the gaseous one. Indeed the ejection of the central object perturbs the gas both in its equilibrium properties and along its trail.

² Note that in this case the noise is given by the emission of the host galaxy itself.

The BH triggers the formation of a density core on the scale of a few r_{inf} , resulting from its sudden removal at the time of its ejection and from the kinetic energy deposition that continue eroding the central density over the whole orbital decay. Along its path, the BH imprints in the gas peculiar features that help to reveal its presence while travelling across its host. The strength of these features depends not only by the ejection velocity, but also on the BH mass and thus on the relationship between a hole and its host. When the motion is subsonic, the BH is surrounded by a nearly spherical distribution of gas particles, resulting in an enhancement of the underlying bremsstrahlung X-ray emission. For the lighter BH (on the $M_{\text{BH}} - M_{\text{bulge}}$ relation), the X-ray feature is visible out to the distance of Virgo. When the motion is supersonic, the BH shocks the gas exciting a conical density and temperature perturbation (the Mach cone), but the enhancement does not lead to a detectable X-ray signal. By contrast, an exceptionally massive BH (above the $M_{\text{BH}} - M_{\text{bulge}}$ relation) carries features that are not only more intense and detectable in a larger cosmic volume, but that also have a unique flavour: the Mach cone is clearly recognisable in X-ray maps with an increase in surface brightness by a factor 2-3 over the background. Therefore, detection of the Mach cone becomes of twofold importance: i) as a probe of high-velocity recoils and ii) as an assessment of the scatter of the $M_{\text{BH}} - M_{\text{bulge}}$ relation at large BH masses. The different shapes in the disturbance can thus in principle help in constraining the extent of the gravitational wave recoil and the scatter in scale relationship between BH masses and their hosts.

The lifetime of the different features correlates with their shape. For initially low Mach numbers, the spherical over-density surrounding the BH, appears every apocentres (i.e. where the BH resides most) where the density contrast is the highest. This signature lasts up to a hundred Myr. For initially high Mach numbers, the Mach cone, recognisable during supersonic passages through the centre, is shorter lived. Despite its longer duration, the subsonic modes carries less information as it can be created either by an initially fastly moving BH once its orbit has decayed, or by an initially slow BH.

It is important to notice that the X-ray features recognised in this work are not due to the direct emission from the BH but only to the perturbed large-scale hot gas of the underlying galaxy. In addition to this, the BH itself can produce its own optical and X-ray emission if it is able to retain a punctured accretion disc at the moment of its ejection from the centre, as suggested by Loeb (2007) (and studied in a statistical context by Volonteri & Madau 2008). The kicked BH in this case can turn on as a displaced QSO/AGN, and a key manifestation of a large recoil should be imprinted in the line systems shifted in velocity from the host galaxies (Bonning et al. 2007). This off-nuclear QSO emission can coexist with the large scale emission features studied in this paper. The contemporary observation of a set of off-set lines and a Mach cone can potentially provide information on the tangential and radial velocities resulting from the kick. Off-centered flares occurring from tidal disruption of bound stars or from marginally bound gas that infall on the disc, can also be present during the lifetime of the recoiling BH (O’Leary & Loeb 2008; Merritt et al. 2008; Shields & Bonning 2008).

The electromagnetic signature of a recoiling BH, de-

tailed in this paper, is different from the one expected in the immediate vicinity of a coalescence event. Electromagnetic afterglows of *LISA* coalescence events (Milosavljević & Phinney 2005; Dotti et al. 2007; Kocsis & Loeb 2008) have peculiar off-on time dependent features varying on much shorter times and spatial scales.

The detectability of X-ray features favours heavier BHs as the strength of the perturbation increases with M_{BH} . Accordingly, the observability is strongly biased toward more massive ellipticals. Interestingly, these massive BHs are out of the *LISA* frequency sensitivity, so that this study would complement our knowledge of gravitational wave in-spiral events in a window not accessible to *LISA*. Massive ellipticals could be the preferred sites where coalescing BHs are expected to get the largest kick ever, due to the lack of a mechanism able to align the two spins prior to the merger (Bogdanović et al. 2007). The discovery of a prominent X-ray feature in the form of a Mach cone will in principle support the idea that high velocity recoils are allowed in environments where a cool dissipative gaseous component is absent.

ACKNOWLEDGEMENTS

We wish to thank Stuart Shapiro and Martin Elvis for fostering the research that led to this paper and Renato Dupke and Lea Giordano for useful discussions. MV and ER acknowledge support from NASA under the Chandra award GO7-8138C and through Chandra Postdoctoral Fellowship grant number PF6-70042 awarded by the Chandra X-ray Center, which is operated by the Smithsonian Astrophysical Observatory for NASA under contract NAS8-03060. BD and MD thank Luca Paredi for technical support. Simulations were performed on the Yoda cluster at the University of Como. BD thanks for the hospitality the Astronomy Department of University of Michigan and MC thanks the hospitality of the Aspen Center for Physics, where part of the study was discussed.

REFERENCES

- Armitage, P.J., Natarajan, P. 2002, *ApJ*, 567, L9
- Baker, J. G., Boggs, W. D., Centrella, J., Kelly, B. J., McWilliams, S. T., Miller, M. C., van Meter, J. R. 2008, *ArXiv e-prints*, 802, arXiv:0802.0416
- Baker, J. G., Boggs, W. D., Centrella, J., Kelly, B. J., McWilliams, S. T., Miller, M. C., van Meter, J. R. 2007, *ApJ*, 668, 1140
- Berczik, P., Merritt, D., Spurzem, R., Bischof, H.-P. 2006, *ApJ*, 624, L21
- Bogdanović, T., Reynolds, C. S., & Miller, M. C. 2007, *ApJ*, 661, L147
- Bonning, E. W., Shields, G. A., & Salviander, S. 2007, *ApJ*, 666, L13
- Boylan-Kolchin, M., Ma, C.-P., & Quataert, E. 2004, *ApJ*, 613, L37
- Bruegmann, B., Gonzalez, J., Hannam, M., Husa, S., & Sperhake, U. 2007, *ArXiv e-prints*, 707, arXiv:0707.0135
- Campanelli, M., Lousto, C., Zlochower, Y., & Merritt, D. 2007, *ApJ*, 659, L5
- Campanelli, M., Lousto, C. O., Zlochower, Y., & Merritt, D. 2007, *Physical Review Letters*, 98, 231102

- Conselice, C. J. 2003, *ApJS*, 147, 1
- Decarli, R., Gavazzi, G., Arosio, I., Cortese, L., Boselli, A., Bonfanti, C., & Colpi, M. 2007, *MNRAS*, 381, 136
- Dotti, M., Colpi, M., Haardt, F., & Mayer, L. 2007, *MNRAS*, 379, 956
- Dotti, M., Salvaterra, R., Sesana, A., Colpi, M., & Haardt, F. 2006, *MNRAS*, 372, 869
- Dotti, M., Colpi, M., & Haardt, F. 2006, *MNRAS*, 367, 103
- Escala, A., Larson, R. B., Coppi, P. S., & Mardones, D. 2005, *ApJ*, 630, 152
- Escala, A., Larson, R. B., Coppi, P. S., & Mardones, D. 2004, *ApJ*, 607, 765
- Favata, M., Hughes, S. A., & Holz, D. E. 2004, *ApJ*, 607, L5
- Ferrarese, L., & Merritt, D. 2000, *ApJ*, 539, L9
- Gardini, A., Rasia, E., Mazzotta, P., Tormen, G. and De Grandi, S., & Moscardini, L. 2004, *MNRAS*, 351, 505
- Gebhardt, K., et al. 2000, *ApJ*, 539, L13
- Gualandris, A., & Merritt, D. 2007, *ArXiv e-prints*, 708, arXiv:0708.0771
- Häring, N., & Rix, H. W. 2004, *ApJL*, 604, L89
- Herrmann, F., Hinder, I., Shoemaker, D. M., Laguna, P., & Matzner, R. A. 2007, *Phys. Rev. D*, 76, 084032
- Herrmann, F., Hinder, I., Shoemaker, D., & Laguna, P. 2007, *Classical and Quantum Gravity*, 24, 33
- Herrmann, F., Hinder, I., Shoemaker, D., Laguna, P., & Matzner, R. A. 2007, *ApJ*, 661, 430
- Hernquist, L. 1990, *ApJ*, 356, 359
- Hopkins, P. F., Hernquist, L., Cox, T. J., Di Matteo, T., Robertson, B., & Springel, V. 2006, *ApJs*, 163, 1
- Hudson, D. S., Reiprich, T. H., Clarke, T. E., & Sarazin, C. L. 2006, *AAp*, 453, 433
- Kocsis, B., & Loeb, A. 2008, *Physical Review Letters*, 101, 041101
- Koppitz, M., Pollney, D., Reisswig, C., Rezzolla, L., Thornburg, J., Diener, P., & Schnetter, E. 2007, *Physical Review Letters*, 99, 041102
- Lauer, T. R., et al. 2007, *ApJ*, 662, 808
- Lippai, Z., Frei, Z., & Haiman, Z. 2008, *ApJL*, 676, L5
- Loeb, A. 2007, *Physical Review Letters*, 99, 041103
- Magorrian, J., et al. 1998, *ApJ*, 115, 2285
- Mayer, L., Kazantzidis, S., Madau, P., Colpi, M., Quinn, T., & Wadsley, J. 2007, *Science*, 316, 1874
- Merritt, D., Milosavljević, M., Favata, M., Hughes, S. A., & Holz, D. E. 2004, *ApJ*, 607, L9
- Merritt, D., Schnittman, J. D., & Komossa, S. 2008, *arXiv:0809.5046*
- Merritt, D., & Milosavljević, M. 2005, *Living Reviews in Relativity*, 8, 8
- Milosavljević, M., Merritt, D. 2001, *ApJ*, 563, 34
- Milosavljević, M. & Phinney, E. S. 2005, *ApJ*, 622, L93
- O'Leary, R. M., & Loeb, A. 2008, *arXiv:0809.4262*
- Ostriker, E. C. 1999, *ApJ*, 513, 252
- Owen, F. N., Odea, C. P., Inoue, M., & Eilek, J. A. 1985, *ApJ*, 294, L85
- Pretorius, F. 2007, *ArXiv e-prints*, 710, arXiv:0710.1338
- Rasia, E., Mazzotta, P., Bourdin, H., Borgani, S., Tornatore, L., Ettori, S., Dolag, K., & Moscardini, L. 2008, *ApJ*, 674, 728
- Richstone, D., et al. 1998, *Nature*, 395, A14
- Rodriguez, C., Taylor, G. B., Zavala, R. T., Peck, A. B., Pollack, L. K., & Romani, R. W. 2006, *ApJ*, 646, 49
- Sesana, A., Haardt, F., & Madau, P. 2007, *ApJ*, 660, 546
- Schnittman, J. D., & Buonanno, A. 2007, *ApJ*, 662, L63
- Schnittman, J. D., & Krolik, J. H. 2008, *ArXiv e-prints*, 802, arXiv:0802.3556
- Shen, S., Mo, H. J., White, S. D. M., Blanton, M. R., Kauffmann, G., Voges, W., Brinkmann, J., & Csabai, I. 2003, *MNRAS*, 343, 978
- Shields, G. A., & Bonning, E. W. 2008, *ArXiv e-prints*, 802, arXiv:0802.3873
- Springel, V., Yoshida, N., & White, S. D. M. 2001, *New Astronomy*, 6, 79
- Tundo, E., Bernardi, M., Hyde, J. B., Sheth, R. K., & Pizzella, A. 2007, *ApJ*, 663, 53
- Volonteri, M., Haardt, F., & Madau, P. 2003, *ApJ*, 582, 559
- Volonteri, M. 2007, *ApJ*, 663, L5
- Volonteri, M., & Madau, P. 2008, *arXiv:0809.4007*
- Yu, Q. 2002, *MNRAS*, 331, 931